

# Hardware-Guided Symbiotic Training for Compact, Accurate, yet Execution-Efficient LSTM

Hongxu Yin, Guoyang Chen, Yingmin Li, Shuai Che, Weifeng Zhang, and Niraj K. Jha, *Fellow, IEEE*

**Abstract**—Many long short-term memory (LSTM) applications need fast yet compact models. Neural network compression approaches, such as the grow-and-prune paradigm, have proved to be promising for cutting down network complexity by skipping insignificant weights. However, current compression strategies are mostly hardware-agnostic and network complexity reduction does not always translate into execution efficiency. In this work, we propose a hardware-guided symbiotic training methodology for compact, accurate, yet execution-efficient inference models. It is based on our observation that hardware may introduce substantial non-monotonic behavior, which we call the latency hysteresis effect, when evaluating network size vs. inference latency. This observation raises question about the mainstream smaller-dimension-is-better compression strategy, which often leads to a sub-optimal model architecture. By leveraging the hardware-impacted hysteresis effect and sparsity, we are able to achieve the symbiosis of model compactness and accuracy with execution efficiency, thus reducing LSTM latency while increasing its accuracy. We have evaluated our algorithms on language modeling and speech recognition applications. Relative to the traditional stacked LSTM architecture obtained for the Penn Treebank dataset, we reduce the number of parameters by  $18.0\times$  ( $30.5\times$ ) and measured run-time latency by up to  $2.4\times$  ( $5.2\times$ ) on Nvidia GPUs (Intel Xeon CPUs) without any accuracy degradation. For the DeepSpeech2 architecture obtained for the AN4 dataset, we reduce the number of parameters by  $7.0\times$  ( $19.4\times$ ), word error rate from 12.9% to 9.9% (10.4%), and measured run-time latency by up to  $1.7\times$  ( $2.4\times$ ) on Nvidia GPUs (Intel Xeon CPUs). Thus, our method yields compact, accurate, yet execution-efficient inference models.

**Index Terms**—Deep learning; grow-and-prune synthesis; language modeling; long short-term memory; neural network; speech recognition; stacked architecture.



## 1 INTRODUCTION

Long short-term memory (LSTM) has been widely deployed for applications like speech recognition [1], neural machine translation [2], health monitoring [3], and language modeling [4], [5]. It is capable of learning both the long-term and short-term dependencies in sequential data [6]. Researchers have kept increasing the depth and size of LSTM models to improve their accuracy. For example, the DeepSpeech2 architecture [1] is more than  $2\times$  deeper and  $10\times$  larger than the initial DeepSpeech architecture [7]. A deep neural network (NN) architecture allows the model to capture low/mid/high-level features through a multi-level abstraction that typically results in high inference accuracy [8]. But it also leads to a sharp increase in computation, thus posing significant challenges to model deployment. In addition, a large NN model consumes substantial storage, memory bandwidth, and computational resources that may be too excessive for mobile and embedded devices [9], [10], [11], [12]. Furthermore, the increasingly stringent latency constraints imposed by real-time applications make large high-latency LSTMs unusable. Thus, it is practically important to optimize the model from all three aspects of performance simultaneously: model compactness, accuracy, and execution efficiency.

Network compression has emerged as a promising technique to reduce the computational cost of deep NNs by eliminating connections with insignificant weights, such as zeros or near-zeros. By leveraging effective network growth [13] and pruning [14] techniques, the number of parameters can be cut down by over  $30\times$  for convolutional neural networks (CNNs) [13], [14], [15] and more than  $10\times$  for LSTMs [5], [16], [17], [18]. However, current compression strategies are mostly hardware-agnostic, and network complexity reduction does not always translate into execution efficiency and may even have an adverse impact on other performance metrics. For example, training NNs towards extreme weight sparsity offers little execution performance gain on current GPUs due to a lack of effective sparsity support. Moreover, some compressed networks may even suffer from inefficient execution, as observed in [19].

In this work, we propose a novel hardware-guided symbiotic training methodology based on our observation that the hardware may introduce substantial non-monotonicity (we call this the *latency hysteresis effect (LHE)*): a smaller model, which typically has a lower accuracy, may also be slower at run-time. This observation raises a question about the mainstream smaller-dimension-is-better strategy, which often leads to a sub-optimal design point in the model architecture space. By leveraging the hardware-impacted hysteresis effect, we are able to achieve the symbiosis of all three performance aspects: higher accuracy, smaller model size, and lower inference latency. To evaluate this symbiotic

---

Hongxu Yin and Niraj K. Jha are with the Department of Electrical Engineering, Princeton University, Princeton, NJ, 08544 USA, e-mail: {hongxuy, jha}@princeton.edu. Guoyang Chen, Yingmin Li, Shuai Che, and Weifeng Zhang are with Alibaba Group US Inc., Sunnyvale, CA, 94085 USA, e-mail: {g.chen, yingmin.li, shuai.che, weifeng.z}@alibaba-inc.com.

strategy, we adopt the internally deeper hidden-layer LSTM (H-LSTM) structure [18] to reduce the number of stacked layers, and start training from a sparse seed architecture, which grows effective connections to reach an initial high accuracy. Then we employ our hardware-guided structured grow-and-prune algorithms to shrink the network into hardware-favored dimensions. Finally, we prune the network weights again for extra compactness.

The major contributions of our approach can be summarized as follows:

- 1) We propose a novel training methodology to exploit hardware LHE to achieve a symbiosis of model compactness and accuracy with reduced run-time latency.
- 2) We combine multi-granular grow-and-prune algorithms with hardware guidance to reduce the model into a hardware-favored architecture. This is the first work that effectively avoids sub-optimal design points that may consume as much as 90% of the model architecture space.
- 3) The reported results outperform those from the literature from all three design perspectives: (a)  $7.0\times$  to  $30.5\times$  model compression, (b) higher accuracy, and (c)  $1.4\times$  to  $5.2\times$  reduction in run-time latency on Nvidia GPUs and Intel Xeon CPUs. Thus, our method yields compact, accurate, yet execution-efficient inference models.

The rest of this paper is organized as follows. We review related works in Section 2. Then, we explain the motivation of this work in Section 3. In Section 4, we discuss our proposed methodology in detail. We present our experimental results on both language modeling and speed recognition in Section 5. Finally, we draw a conclusion in Section 6.

## 2 RELATED WORK

Various attempts have been made to improve the efficiency of LSTM models. One direction focuses on improving the LSTM cells. The gated recurrent unit (GRU) utilizes reset and update gates to achieve a similar performance to an LSTM while reducing computational cost [20]. Quasi-RNN explores the intrinsic parallelism of time series data to outperform an LSTM for the same hidden state width [21]. H-LSTM incorporates deeper control gates to reduce the number of external stacked layers. It achieves higher accuracy than the GRU and LSTM with fewer parameters [18].

Network compression techniques, such as the grow-and-prune paradigm, have recently emerged as another direction for reducing LSTM redundancy. The pruning method was initially shown to be effective on large CNNs by demonstrating the reduction in the number of parameters in AlexNet by  $9\times$  and VGG by  $13\times$  for the well-known ImageNet dataset, without any accuracy loss [14]. Follow-up works have successfully scaled this technique to LSTMs [5], [16], [17]. For example, a recent work proposes structured pruning for LSTMs through group LASSO regularization [5]. Network growth is a complementary method to pruning. It enables a more sparse yet accurate model to be obtained before pruning starts [13]. A grow-and-prune paradigm typically reduces the number of parameters in

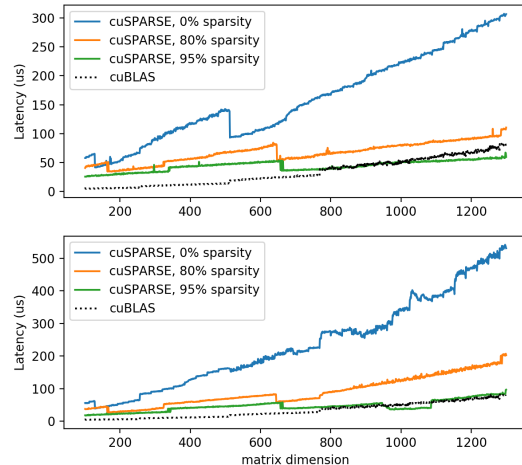


Fig. 1. Matrix multiplication latency on Nvidia Tesla P100 (up) and Quadro P2000 (down) GPUs using cuSPARSE and cuBLAS libraries. Weight matrix: sparse and square, dimension on the  $x$ -axis. Input matrix: dense, batch size 16.

CNNs [13] and LSTMs [18] by another  $2\times$ . However, all these methods are hardware-agnostic. Most of them utilize monotonic optimization metrics, e.g., smaller matrix dimensions or fewer multiply-accumulate operations, hence optimize towards slimmer or more sparse models that may not necessarily translate into execution efficiency.

There have been some recent efforts towards bridging the gap between complexity removal and execution efficiency for CNNs through hardware-heuristics-guided pruning approaches. For example, Scalpel [19] adopts different pruning strategies based on three hardware parallelism levels (low, moderate, and high) of the underlying hardware. DeftNN [22] removes a synapse vector that is highly correlated with another one in the weight matrix, on the assumption that a smaller dimension leads to improved latency. However, both works are based on high-level hardware heuristics rather than real hardware behavior like LHE, which may lead to sub-optimal networks. Energy-aware pruning [23] adopts a hardware energy consumption model in its pruning criteria. However, it leads to a re-design for each target hardware and requires expert knowledge of the hardware. Thus, it is not very user-friendly. Chameleon [24] can effectively adapt CNNs to target platforms and deliver ChamNets that achieve consistent accuracy gains across various latency constraints relative to MobileNetV2 [25], MnasNet [26], and ShuffleNetV2 [27]. However, construction of Chameleon’s three predictors may require training hundreds of baseline models, hence may be time-consuming. In the domain of recurrent NNs, a relevant work explores hardware-inspired weight- and block-level sparsity for speech recognition [28]. With cuSPARSE library support, it delivers  $0.8\times$  to  $4.5\times$  speed-up relative to the dense baseline. However, we find cuSPARSE [29] to be slower than the latest cuBLAS [30] dense library for matrix multiplication, which is a key operation in LSTM. In Fig. 1, we compare these two libraries on GPUs over a typical dimension range of LSTMs. It can be observed that

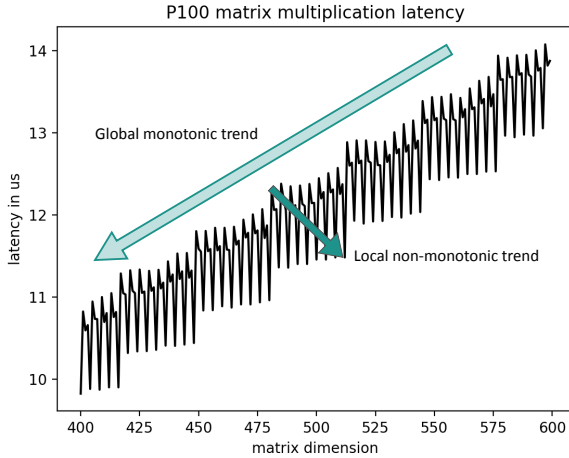


Fig. 2. Example of non-monotonicity in matrix multiplication on the Nvidia Tesla P100 GPU. The weight matrix is square with its dimension on the  $x$ -axis. The input has a batch size of 16.

cuSPARSE is slower than cuBLAS even at a 95% sparsity level.

### 3 MOTIVATION

As opposed to most prior works that use floating-point operations (FLOPs) or multiply-and-accumulate (MAC) operations as an indirect metric for evaluating model compactness, we aim to develop an automated LSTM synthesis flow that acts on directly measured inference latency. This flow does not adopt the traditional assumption that a smaller model (e.g., with smaller hidden state widths) is implicitly faster. In fact, we show that such an assumption is often not valid at run-time on hardware. This points to the need for a new methodology that can link model simplification algorithms to direct execution benefits.

Let us first profile the latency of the matrix multiplication operation on a GPU, as shown in Fig. 2, due to its computational importance. This operation consumes more than half of the computational time in LSTMs. We observed two distinct trends when considering matrix dimension vs. latency:

- 1) Global monotonic trend: a smaller dimension is, in general, faster in terms of run-time latency due to the reduced number of weights (i.e., computation).
- 2) Local non-monotonic trend: the run-time latency lags behind or even reverts the trend as the weight dimension decreases. We refer to this local trend as LHE and the point where LHE starts to occur as the latency hysteresis point (LHP). Within the latency hysteresis bin (i.e., the local range), smaller dimensions worsen run-time latency relative to the corresponding LHP.

LHE is caused by cache line granularity when loading/storing data and vectorization optimization (e.g., vectorized vs. general matrix multiplication kernels) enabled at some particular data input dimensions to take full advantage of the bus bandwidth and single-instruction-multiple-data (SIMD) nature of hardware processing units. Change

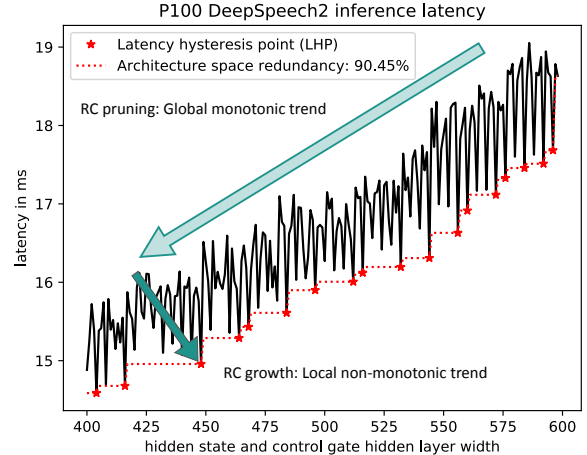


Fig. 3. Inference latency per test instance for the DeepSpeech2 architecture on the Nvidia Tesla P100 GPU. The hidden state and control gate hidden layer widths are set to the same number. The input has a batch size of 16. Architecture space redundancy:  $(1 - \text{\#LHPs} / \text{\#total design points}) \times 100\%$ . RC: row/column.

of optimization strategies for memory placement or computation scheduling can easily impact the final execution efficiency for inference [31], [32]. This also leads to a pervasive presence of LHE on a CPU.

The impact of LHE can scale up to the inference model level. For example, Fig. 3 shows a plot of the DeepSpeech2 inference latency against model size (specified by the hidden state width and the control gate hidden layer width). We can observe that a smaller DeepSpeech2 architecture, which also typically has a lower accuracy, may also be slower in runtime. This raises a question about the mainstream smaller-is-better strategy, given the existence of a large number of LHPs that make more than 90% of the design points in Fig. 3 sub-optimal.

### 4 METHODOLOGY

In this work, we combine the multi-granular grow-and-prune algorithms with network profiling to optimize the network towards a joint algorithm-hardware optimal solution. We summarize our main synthesis flow in Fig. 4. The proposed synthesis process starts with a partially connected seed architecture. Under the guidance of hardware profiles, the multi-granularity of our algorithms enables the network to adaptively expand (row/column growth), shrink (row/column pruning), condense (weight growth), and sparsify (weight pruning) into hardware-favored design points. This benefits hardware even when there is no sparsity support. In the final stage, the synthesis flow rests at a compact design point that is both compact and hardware friendly.

We illustrate the details of our training methodology in Fig. 5. As shown in its upper section, we adopt the H-LSTM cell that adds hidden layers to its control gates [18]. Its internal computation flow is governed by the following equations:

$$\begin{pmatrix} \mathbf{f}_t \\ \mathbf{i}_t \\ \mathbf{o}_t \\ \mathbf{g}_t \end{pmatrix} = \begin{pmatrix} \text{NN}_f([\mathbf{x}_t, \mathbf{h}_{t-1}]) \\ \text{NN}_i([\mathbf{x}_t, \mathbf{h}_{t-1}]) \\ \text{NN}_o([\mathbf{x}_t, \mathbf{h}_{t-1}]) \\ \text{NN}_g([\mathbf{x}_t, \mathbf{h}_{t-1}]) \end{pmatrix} = \begin{pmatrix} \sigma(\mathbf{W}_f H^*([\mathbf{x}_t, \mathbf{h}_{t-1}]) + \mathbf{b}_f) \\ \sigma(\mathbf{W}_i H^*([\mathbf{x}_t, \mathbf{h}_{t-1}]) + \mathbf{b}_i) \\ \sigma(\mathbf{W}_o H^*([\mathbf{x}_t, \mathbf{h}_{t-1}]) + \mathbf{b}_o) \\ \tanh(\mathbf{W}_g H^*([\mathbf{x}_t, \mathbf{h}_{t-1}]) + \mathbf{b}_g) \end{pmatrix}$$

$$\mathbf{c}_t = \mathbf{f}_t \otimes \mathbf{c}_{t-1} + \mathbf{i}_t \otimes \mathbf{g}_t$$

$$\mathbf{h}_t = \mathbf{o}_t \otimes \tanh(\mathbf{c}_t)$$

where  $\mathbf{f}_t$ ,  $\mathbf{i}_t$ ,  $\mathbf{o}_t$ ,  $\mathbf{g}_t$ ,  $\mathbf{x}_t$ ,  $\mathbf{h}_t$ , and  $\mathbf{c}_t$  denote the forget gate, input gate, output gate, cell update vector, input, hidden state, and cell state at step  $t$ , respectively;  $\mathbf{h}_{t-1}$  and  $\mathbf{c}_{t-1}$  refer to the previous hidden and cell states at step  $t-1$ ;  $\text{NN}$ ,  $H$ ,  $\mathbf{W}$ ,  $\mathbf{b}$ ,  $\sigma$ , and  $\otimes$  refer to NN gates, hidden layer that performs a linear transformation followed by an activation function, weight matrix, bias, *sigmoid* function, and element-wise multiplication, respectively;  $*$  indicates zero or more  $H$  layers for each NN gate.  $H$  layers offer three advantages. First, they enhance gate control through a multi-level abstraction, hence alleviate H-LSTM's reliance on external stacking. Second, they can be easily regularized through dropout, and thus lead to better generalization. Third, they offer a wide range of choices for internal activation functions, such as the ReLU. This may provide additional benefits, such as faster learning and computation reduction due to zero outputs [18].

We utilize four training steps to learn the values, connectivity, and dimensions of the NN gates in the H-LSTM. We show these steps in the lower part of Fig. 5. Training starts from a sparse seed architecture that contains a small fraction of connections to facilitate the initial back propagation of gradient information. During the weight growth (wg) phase, it iteratively wakes up only the most effective connections to reach high accuracy based on the gradient information. Then, it uses structured row/column pruning (rcp) algorithms to shrink the network dimensions, leading to lower inference latency. Next, it profiles the latency model on hardware and uses row/column growth (rcg) algorithms to obtain a network from LHE-aware locally optimal design points. This enables simultaneous latency and accuracy gains, as shown later. Finally, it prunes away some weights for extra compactness.

We next explain in detail the algorithms involved in these four steps. Unless otherwise stated, we assume a mask-based approach for tackling sparse networks. Each weight matrix  $\mathbf{W}$  has a corresponding binary mask matrix  $\mathbf{Msk}$  that is of the exact same size. We finally update each  $\mathbf{W}$  with its corresponding  $\mathbf{W} \otimes \mathbf{Msk}$  after the training flow terminates.

#### 4.1 Weight growth & pruning

The main objective of the weight growth phase is to locate only the most effective dormant connections to reduce the value of the loss function  $L$ . We first evaluate  $\partial L / \partial w$  for each dormant connection  $w$  based on its average gradient over the entire training set. Then, we activate a dormant connection based on the following policy:

$$\mathbf{Msk}(w) = 1, \text{ iff } |w \cdot \text{grad}| \geq (100(1 - g_w))^{th} \text{ percentile of } |\mathbf{W} \cdot \text{grad}|$$

where  $g_w$  denotes the weight growth ratio. This rule was first proposed in [13]. It caters to dormant connections that are most efficient at loss function  $L$  reduction, and enables the network to reach a target accuracy with far less

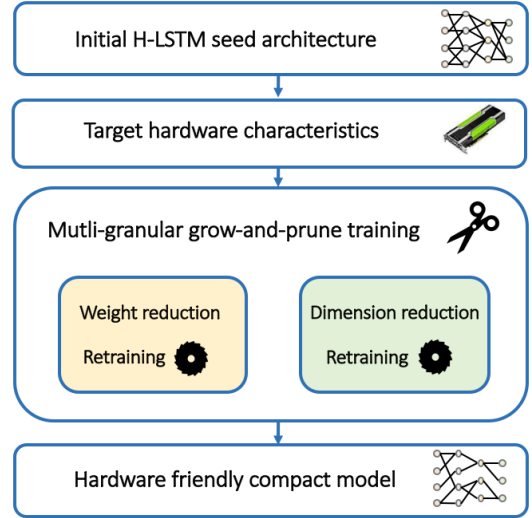


Fig. 4. An illustration of the hardware-aware architecture synthesis flow.

redundancy than a fully connected model. This offers an accurate yet irredundant model for all the subsequent steps to act on.

We adopt the magnitude-based weight pruning strategy for final redundancy removal. Pruning of insignificant weights is an iterative process. In each iteration, we adopt the following policy for weight selection:

$$\mathbf{Msk}(w) = 0, \text{ iff } |w| \leq (100p_w)^{th} \text{ percentile of } |\mathbf{W}|$$

where  $p_w$  denotes the weight pruning ratio. We prune a neuron if all its input (or output) connections are pruned away. We retrain the network after the weight pruning iteration to recover its performance. The pruning phase terminates when retraining cannot achieve a pre-defined accuracy threshold. In the final training step, weight pruning minimizes the memory requirement of the final inference model. It also provides a high weight sparsity level for sparsity-driven libraries, such as Intel Math Kernel Library (MKL) [33] on Intel CPUs, as shown later.

#### 4.2 Row/column growth & pruning

The grow-and-prune approach at the row/column level enables the network to adaptively expand and shrink its dimensions. This leads to an effective descent in the model architecture space towards fast, accurate, yet execution-efficient design points. However, due to the introduction of a large number of sub-optimal design points by hardware, the model architecture space may become rather non-monotonic, thus necessitating a carefully-crafted stopping criterion for this process.

We propose row/column grow-and-prune algorithms to exploit LHE for hardware-symbiotic solutions. The pruning algorithm takes advantage of the global trend to shrink the model dimension for latency reduction, whereas the growth algorithm recovers the model back to its corresponding LHP for simultaneous latency and accuracy gains.

We present the row/column pruning algorithm in Algorithm 1. Inspired by magnitude-based weight pruning methods, we examine the sum of the magnitudes of the weights

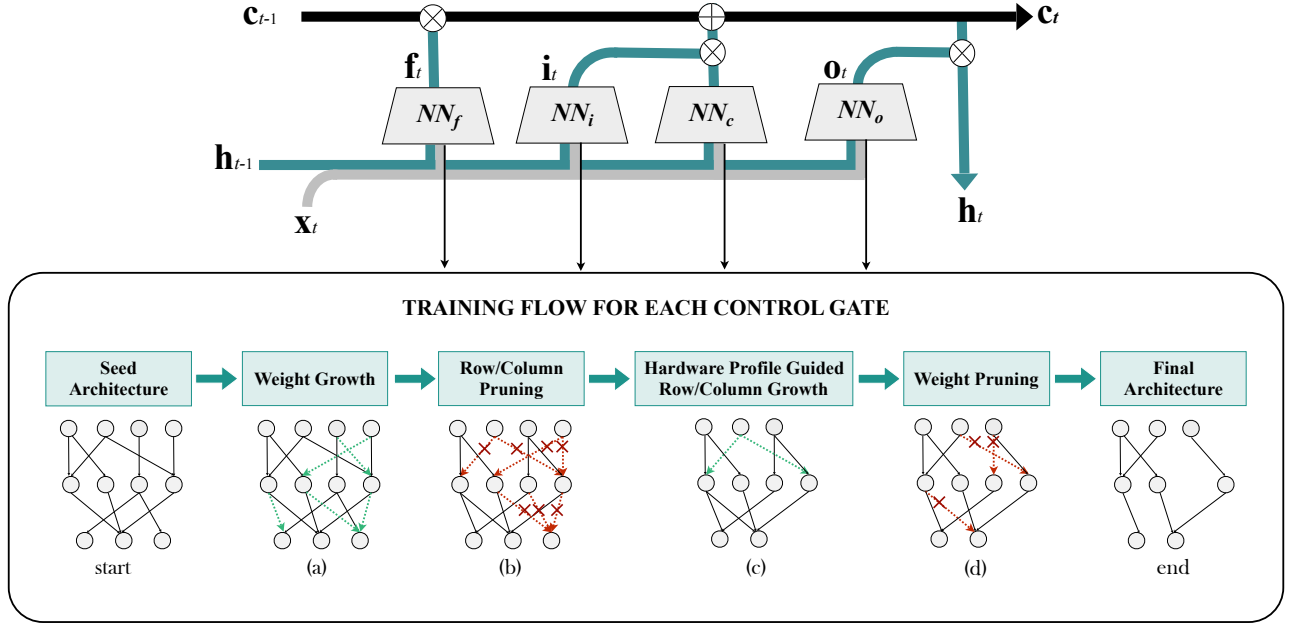


Fig. 5. Schematic diagram of our training methodology.

#### Algorithm 1 Row/column pruning algorithm

**Input:**  $p_c$  - column pruning ratio,  $p_r$  - row pruning ratio,  $\mathbf{W} \in R^{M \times N}$  - control gate tensor,  $\mathbf{Msk} \in R^{M \times N}$  - mask tensor  
**Denote:**  $M$  - row count,  $N$  - column count  
 $thr = (p_r N)^{th}$  smallest value in  $sum(abs(\mathbf{W}), axis = 1)$   
 $thc = (p_c M)^{th}$  smallest value in  $sum(abs(\mathbf{W}), axis = 0)$   
**for**  $1 \leq m \leq M$  **do**  
  **if**  $sum(abs(\mathbf{W}_{m,:})) \leq thc$  **then**  
     $\mathbf{Msk}_{m,:} = 0$   
     $\mathbf{W}_{m,:} = 0$   
  **end if**  
**end for**  
**for**  $1 \leq n \leq N$  **do**  
  **if**  $sum(abs(\mathbf{W}_{:,n})) \leq thr$  **then**  
     $\mathbf{Msk}_{:,n} = 0$   
     $\mathbf{W}_{:,n} = 0$   
  **end if**  
**end for**

per row/column for importance ranking. Row/column pruning is also an iterative process. We retrain the network after each pruning iteration, and stop if retraining cannot recover the performance to a pre-defined accuracy threshold.

Algorithm 2 illustrates our gradient-based row/column growth algorithm. Similar to the weight growth algorithm, we first evaluate  $\partial L / \partial w$  for all the dormant connections in the network based on the average gradient over the entire training set (or a large batch). We only wake up the dormant rows and columns that possess the largest gradient magnitude sums, hence yielding the most efficiency in the reduction of loss function  $L$ .

## 5 EXPERIMENTAL RESULTS

We next present our experimental results for the language modeling and speech recognition benchmarks. We imple-

#### Algorithm 2 Row/column growth algorithm

**Input:**  $g_c$  - column growth ratio,  $g_r$  - row growth ratio,  $\mathbf{W} \in R^{M \times N}$  - control gate tensor,  $\mathbf{Msk} \in R^{M \times N}$  - mask tensor  
**Denote:**  $M$  - row count,  $N$  - column count,  $\mathbf{G} \in R^{M \times N}$  - bridging gradient matrix,  $set_c$  - indices for existing columns,  $set_r$  - indices for existing rows,  $lr$  - current learning rate  
**for**  $1 \leq m \leq M, 1 \leq n \leq N$  **do**  
  **if**  $m$  in  $set_c$  **and**  $n$  in  $set_r$  **then**  
     $\mathbf{G}_{m,n} = 0$   
  **end if**  
**end for**  
 $thr = (g_r N)^{th}$  largest value in  $sum(abs(\mathbf{G}_{:,set_c}), axis = 1)$   
 $thc = (g_c M)^{th}$  largest value in  $sum(abs(\mathbf{G}_{set_r,:}), axis = 0)$   
**for**  $1 \leq m \leq M$  **do**  
  **if**  $sum(abs(\mathbf{G}_{m,set_c})) \geq thr$  **then**  
     $\mathbf{Msk}_{m,set_c} = 1$   
     $\mathbf{W}_{m,set_c} = \mathbf{G}_{m,set_c} \cdot lr$   
  **end if**  
**end for**  
**for**  $1 \leq n \leq N$  **do**  
  **if**  $sum(abs(\mathbf{G}_{set_r,n})) \geq thc$  **then**  
     $\mathbf{Msk}_{set_r,n} = 1$   
     $\mathbf{W}_{set_r,n} = \mathbf{G}_{set_r,n} \cdot lr$   
  **end if**  
**end for**

ment our methodology using PyTorch [34] on both Nvidia GPUs and Intel Xeon CPUs. For GPU, we have experimented with Nvidia GPUs: Quadro P2000, Tesla P100, and Tesla V100. For CPU, we have targeted Intel Xeon CPUs: Gold 5118 (2.3 GHz), E5-2682 v4 (2.5 GHz), and Broadwell (2.4 GHz). For CPU inference, we use Intel MKL [33] implementations for sparse matrix operation.

TABLE 1  
Performance gain breakdown of each training step for language modeling on GPUs

Step	Model	#Params.	Perplexity	Latency		
				P2000	P100	V100
	Baseline LSTM	14.46M	72.1	3.52ms	2.12ms	2.72ms
(a)	H-LSTM+wg	4.68M	70.2	2.21ms	1.45ms	1.81ms
(b)	H-LSTM+wg+rcp	3.21M	72.2	1.78ms	1.27ms	1.51ms
(c)	H-LSTM+wg+rcp+rcg	3.24M	71.8	1.65ms	1.18ms	1.14ms
(d)	H-LSTM+wg+rcp+rcg+wp	0.80M	72.1	1.65ms	1.18ms	1.14ms

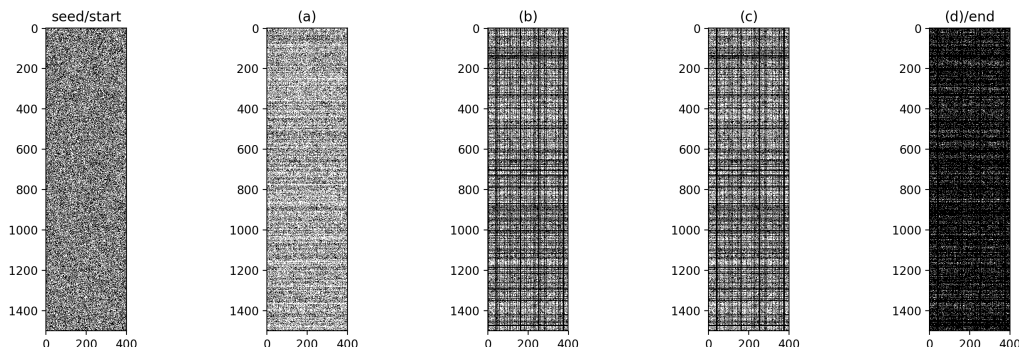


Fig. 6. Change of a typical input-to-hidden-layer weight matrix in the H-LSTM in different phases. White sections denote active connections. All non-zero elements are changed to 1 for better visualization.

## 5.1 Language modeling

We first demonstrate the effectiveness of our approach on language modeling.

**Model architecture:** We experiment with a stacked LSTM architecture for this application that feeds embedded word vectors to the recurrent layers. The word vocabulary has size 10,000. The dimension of the input word embedding is 400. We first train a conventional stacked LSTM architecture as the baseline. It contains two stacked recurrent layers, each with the hidden state width set to 1500, same as in [4], [5], [35]. Next, we implement our methodology on a one-layer H-LSTM with the hidden state width again set to 1500. Each control gate contains one hidden layer with this width.

**Dataset:** We report results on the Penn Treebank (PTB) dataset [36]. It contains 929k, 73k, and 82k words in the training, validation, and test sets, respectively.

**Training:** We use a stochastic gradient descent (SGD) optimizer for this application. We initialize the learning rate to 30, decayed by 10 when the validation accuracy does not increase in 50 consecutive epochs. We use a batch size of 32 for training. We use a dropout ratio of 0.2 for the hidden layers in the control gates, as in [18], 0.65 for input embedding layers, and 0.1 for input words, as in [37]. We employ L2 regularization during training with a weight decay of  $1.2 \times 10^{-6}$ . We use word-level perplexity as our evaluation criterion, same as in [4], [5], [35].

We next present our experimental results for GPU and CPU inference.

### 5.1.1 Synthesized models for GPU inference

We first implement our methodology on various GPUs and compare our results with those for the conventional stacked

LSTM architecture in Table 1. Latency indicates the average value per test word sequence of length 70 over the entire test set at a batch size of 16. It can be observed that the four steps in our learning algorithm work sequentially and collaboratively to learn structured sparsity in the network, as shown in Fig. 6. To further illustrate the performance gains obtained in each training step, we also break down their individual contributions in Table 1, and present the details next:

Step (a): The seed architecture has a 50% sparsity level. In the weight growth phase, we use a growth ratio set to 10% for the first eight epochs. This enables the network to reach a 70.2 perplexity with only 65% of its available connections, i.e., at a 35% sparsity level.

Step (b): We use equal pruning ratios for rows and columns of 20%. We halve the pruning ratios if the post-retraining perplexity surpasses a pre-defined performance threshold. For this application, we set the performance threshold to 72.1. This is the performance achieved by our stacked LSTM model, and better than the values reported in [4], [5], [35], [40]. In the final stage, we iteratively prune away single rows and columns until the performance threshold can no longer be satisfied. This enables us to fully exploit the global monotonic trend for latency reduction. After this step, the dimension of each control gate matrix shrinks from 1500/400 to 1197/317. This brings a 14% to 20% reduction in inference latency.

Step (c): We next locate the LHPs for each GPU before starting the growth process. For this application, we find all three GPUs favor the same 1200/320 LHP in the model architecture space defined by the control gate dimension. We then calculate the growth ratios accordingly to recover the network into this LHP. As expected, LHE exploration

TABLE 2  
Inference model comparison for language modeling on GPUs

Model	#Params.	Perplexity	Latency		
			P2000	P100	V100
Our stacked LSTM - baseline	14.5M	72.1	3.52ms	2.12ms	2.72ms
Sukhbaatar et al. [38]	-	120	-	-	-
Mikolov et al. [39]	-	115/115	-	-	-
Wen et al. [5]	14.9M	78.7	-	-	-
Zhu and Gupta [35]	7.2M	77.5	7.94ms*	3.69ms*	3.02ms*
Zaremba, Sutskever, and Vinyals [40]	18.0M <sup>†</sup>	73.6	-	-	-
Lin et al. [4]	9.0M <sup>†</sup>	72.2	-	-	-
<b>This work</b>	<b>0.80M (18.0×)</b>	<b>72.1</b>	<b>1.65ms (2.1×)</b>	<b>1.18ms (1.8×)</b>	<b>1.14ms (2.4×)</b>

<sup>†</sup>Pessimistic estimate at zero word embedding dimension, i.e. ultimate lower bound, and 1500 hidden state width as reported in the paper.

\* Measured based on our implementation of the exact same configuration as reported in the paper.

enables a 7% to 23% reduction in measured inference latency jointly with a 0.4 perplexity bonus.

Step (d): We use an initial weight pruning ratio of 70% and update it based on the same rule as in Step (b). This step further reduces the number of network parameters by 4.1×.

We compare our final inference model with relevant work in Table 2. Our models outperform the ones in the literature from all three design perspectives. Against the stacked LSTM baseline, we reduce the number of parameters by 18.0×, and measured run-time latency by 2.1×, 1.8×, and 2.4× on Nvidia P2000, P100, and V100 GPUs, respectively, without any accuracy degradation.

### 5.1.2 Synthesized models for CPU inference

We next report results from the implementation of our methodology on CPUs. We base our experiments on the Intel MKL [33] implementation due to its support and acceleration of sparse matrix computations. For CPU inference, we skip the dimension reduction process (i.e., Step(b) and Step(c)) to fully exploit the potential of weight sparsity. The high sparsity level without dimension reduction at 93.4% enables us to fully explore the benefit of sparsity acceleration, as opposed to a sparsity level at 83.5% with dimension reduction that undermines the benefits of MKL. This yields additional 1.6× latency and 2× parameter reduction. Our final model has a test perplexity of 72.1, same as the test perplexity of the LSTM baseline. It only contains 0.47M parameters as opposed to the baseline LSTM model that has 14.5M parameters (leading to a 30.5× compression ratio).

We next compare the latency of the final inference models on CPUs in Table 3. Relative to the LSTM baseline for language modeling, we reduce the inference latency by 76.1% (4.2×), 80.8% (5.2×), and 75.8% (4.1×) on Intel Xeon Gold 5518, E5-2682 v4, and Broadwell CPUs, respectively. Sparsity-driven MKL acceleration contributes approximately 2.5× speed-up, while utilizing H-LSTM cells contributes the remaining 2× speed-up on the CPUs.

## 5.2 Speech recognition

We now consider another well-known application: speech recognition.

**Model architecture:** We implement a bidirectional DeepSpeech2 architecture that employs stacked recurrent layers following the convolutional layers for speech recognition [1]. We extract Mel-frequency cepstral coefficients

from the speech data in a 20ms feature extraction window. There are two CNN layers present prior to the recurrent layers and one connectionist temporal classification layer for decoding [41] after the recurrent layers. The width of the hidden state is 800, same as in [4], [42]. Each control gate contains one hidden layer with width 800.

**Dataset:** We obtain the results for the AN4 dataset [43]. It contains 948 training utterances and 130 testing utterances.

**Training:** We utilize a Nesterov SGD optimizer in our experiment. We use a batch size of 16 for training. We initialize the learning rate to  $3 \times 10^{-4}$  and decay it by 0.99 after every training epoch. We use a dropout ratio of 0.2 for the hidden layers in the H-LSTM. We use batch normalization between recurrent layers. We use L2 regularization with a weight decay of  $1 \times 10^{-4}$ . We use word error rate (WER) as our evaluation criterion, same as in [4], [42], [44].

We adopt the model reported in [4] as our LSTM baseline. It contains five stacked LSTM layers with a hidden state width of 800. Then, we implement our methodology and compare our results for GPU and CPU inference as follows.

### 5.2.1 Synthesized models for GPU inference

We summarize our results for GPU inference in Table 4. Latency values indicate the average instance latency over the test set with a batch size of 16. In Table 4, we also break down the changes in model characteristics throughout the training flow to separate the performance gains at each training step:

Step (a): The seed architecture has a 50% sparsity level. In the weight growth phase, we use a growth ratio of 10% for the first six training epochs. This enables the network to reach an 8.39% WER with only 62% of its available connections, i.e., at a 38% sparsity level.

Step (b): We also adopt equal row and column pruning ratios of 20%, and update them using the same method as in Step (b) of the language modeling application. This trims down the dimension of each weight matrix from 800/800 to 626/626, thus reducing the measured inference latency by 2% to 30% across the three targeted GPUs.

Step (c): Unlike in the case of language modeling, this step unveils different LHPs for the P2000 and P100 GPUs: it recovers the network into a 640/640 LHP for the P2000 GPU and a 644/644 LHP for the P100 GPU. LHE exploration for speech recognition enables an additional 0.22% to 0.85% WER reduction, jointly with a latency reduction of 9.2% to 19.2%.

TABLE 3  
Inference model comparison for language modeling on CPUs

CPU platform	Baseline LSTM latency	This work	Speed-up factor
Intel Xeon E5-2682 v4	115.90ms	22.64ms	5.1×
Intel Xeon Gold 5118	125.08ms	24.02ms	5.2×
Intel Xeon Broadwell	81.03ms	19.57ms	4.1×

TABLE 4  
Performance gain breakdown of each training step for speech recognition on GPUs

GPU platform	Step	Model	#Layers	Dimension	#Params.	WER(%)	Latency
Nvidia P2000		Baseline LSTM [4]	5	800/800	50.4M	12.90	35.87ms*
	(a)	H-LSTM+wg	3	800/800	27.1M	8.39	32.13ms
	(b)	H-LSTM+wg+rcp	3	626/626	18.2M	10.29	22.55ms
	(c)	H-LSTM+wg+rcp+rcg	3	644/644	18.3M	9.44	20.79ms
	(d)	H-LSTM+wg+rcp+rcg+wp	3	644/644	8.1M	9.97	20.79ms
Nvidia P100		Baseline LSTM [4]	5	800/800	50.4M	12.90	24.04ms*
	(a)	H-LSTM+wg	3	800/800	27.1M	8.39	22.77ms
	(b)	H-LSTM+wg+rcp	3	626/626	18.2M	10.30	19.61ms
	(c)	H-LSTM+wg+rcp+rcg	3	640/640	18.3M	10.08	17.70ms
	(d)	H-LSTM+wg+rcp+rcg+wp	3	640/640	7.2M	10.25	17.70ms
Nvidia V100		Baseline LSTM [4]	5	800/800	50.4M	12.90	19.35ms*
	(a)	H-LSTM+wg	3	800/800	27.1M	8.39	17.67ms
	(b)	H-LSTM+wg+rcp	3	626/626	18.2M	10.30	17.32ms
	(c)	H-LSTM+wg+rcp+rcg	3	640/640	18.3M	10.08	13.99ms
	(d)	H-LSTM+wg+rcp+rcg+wp	3	640/640	7.2M	10.25	13.99ms

\* Measured based on our implementation of the exact same configuration as reported in the paper.

TABLE 5  
Inference model comparison for speech recognition on GPUs

Model	#Params.	WER(%)	Latency
	P2000 / P100 / V100	P2000 / P100 / V100	P2000 / P100 / V100
Lin et al. [4] - baseline	50.4M	12.90	35.87ms* / 24.04ms* / 19.35ms*
Alistarh et al. [44]	13.0M	18.85	-
Naren [42]	37.8M	10.52	-
Dai, Yin, and Jha [18]	2.6M	10.37	32.13ms / 22.77ms / 17.67ms
<b>This work</b>	<b>8.1M (6.2×) / 7.2M (7.0×) / 7.2M (7.0×)</b>	<b>9.97 / 10.25 / 10.25</b>	<b>20.79ms (1.7×) / 17.70ms (1.4×) / 13.99ms (1.4×)</b>

Step (d): We initialize the weight pruning ratio to 70% and update it using the same rule as in Step (d) in the language modeling application. This step reduces the number of network parameters by 2.3× to 2.5×.

We compare our final inference models with relevant work in Table 5. Our results outperform most of the previous work from all three design perspectives. Though containing more parameters than the models presented in [18], our models achieve higher accuracy and deliver substantial inference speed-ups. Relative to the conventional LSTM baseline [4], our method reduces the measured inference latency by 1.7× (1.4×/1.4×) on the P2000 (P100/V100) GPU, while simultaneously reducing the number of parameters by 6.2× (7.0×/7.0×), and WER from 12.90% to 9.97% (10.25%/10.25%).

### 5.2.2 Synthesized models for CPU inference

We also exploit weight sparsity for speech recognition on CPUs. Augmented by Intel MKL, weight sparsity offers substantial memory and latency reductions at run-time. Similar to language modeling, we skip the dimension reduction process (i.e., Step(b) and Step(c)) to fully exploit the potential of weight sparsity. The high sparsity level without dimension reduction at 94.2% enables us to fully

exploit sparsity acceleration, as opposed to a sparsity level at 88.8% with dimension reduction that undermines the benefits of MKL. This yields additional 1.4× latency and 2.8× parameter reduction. Our final CPU inference model contains only 2.6M parameters as opposed to the baseline LSTM model that has 50.4M parameters (19.4× compression ratio). It has a WER of 10.37%, which is 2.53% more accurate than the LSTM baseline.

We next compare the latency of the final inference models on the CPUs in Table 6. Relative to the LSTM baseline for speech recognition, we reduce the inference latency by 57.9% (2.4×), 53.8% (2.2×), and 54.8% (2.2×) on Intel Xeon Gold 5518, E5-2682 v4, and Broadwell CPUs, respectively. Sparsity-driven MKL acceleration contributes approximately 2× speed-up, whereas utilizing H-LSTM cells contributes the remaining 1.1× speed-up.

## 6 CONCLUSIONS

In this work, we proposed a hardware-guided symbiotic training methodology for compact, accurate, yet execution-efficient inference models. By leveraging hardware-impacted LHE and multi-granular grow-and-prune algorithms, we were able to reduce LSTM latency while increasing its accuracy. We evaluated our algorithms on the lan-

TABLE 6  
Inference model comparison for speech recognition on CPUs

CPU platform	Baseline LSTM latency	This work	Speed-up factor
Intel Xeon E5-2682 v4	179.0ms	75.3ms	2.4×
Intel Xeon Gold 5118	202.1ms	93.3ms	2.2×
Intel Xeon Broadwell	146.7ms	66.3ms	2.2×

Baseline latency values are measured based on our implementation of the exact same configuration as reported in [4].

guage modeling and speech recognition applications. Relative to the traditional stacked LSTM architecture obtained for the Penn Treebank dataset, we reduced the number of parameters by 18.0×, and measured run-time latency by 2.1×, 1.8×, and 2.4× on the Nvidia P2000, P100, and V100 GPUs, respectively, without any accuracy degradation. We reduced the number of parameters by 30.5×, and measured run-time latency by 5.1×, 5.2×, and 4.1× on the Intel Xeon E5-2682 v4, Gold 5518, and Broadwell CPUs, respectively, without any accuracy degradation. Relative to the DeepSpeech2 architecture obtained from the AN4 dataset, we reduced the number of parameters by 7.0×, WER from 12.9% to 9.9%, and measured run-time latency by 1.7×, 1.4×, and 1.4× on the Nvidia P2000, P100 and V100 GPUs, respectively. We also reduced the number of parameters by 19.4×, WER from 12.9% to 10.4%, and measured run-time latency by 2.4×, 2.2×, and 2.2× on the Intel Xeon E5-2682 v4, Gold 5518, and Broadwell CPUs, respectively. Thus, our method yields compact, accurate, yet execution-efficient inference models.

## REFERENCES

- [1] D. Amodei, R. Anubhai, E. Battenberg, C. Case, J. Casper, B. Catanzaro, J. Chen, M. Chrzanowski, A. Coates, G. Diamos, E. Elsen, J. Engel, L. Fan, C. Fougner, T. Han, A. Hannun, B. Jun, P. LeGresley, L. Lin, S. Narang, A. Ng, S. Ozair, R. Prenger, J. Raiman, S. Satheesh, D. Seetapun, S. Sengupta, Y. Wang, Z. Wang, C. Wang, B. Xiao, D. Yogatama, J. Zhan, and Z. Zhu, "Deep Speech 2 : End-to-End speech recognition in English and Mandarin," in *Proc. Int. Conf. Machine Learning*, vol. 48, 2016, pp. 173–182.
- [2] I. Sutskever, O. Vinyals, and Q. V. Le, "Sequence to sequence learning with neural networks," in *Proc. Advances in Neural Information Processing Systems*, 2014, pp. 3104–3112.
- [3] B. Ballinger, J. Hsieh, A. Singh, N. Sohoni, J. Wang, G. H. Tison, G. M. Marcus, J. M. Sanchez, C. Maguire, J. E. Olgin, and M. J. Pletcher, "DeepHeart: Semi-supervised sequence learning for cardiovascular risk prediction," in *Proc. AAAI Conf. Artificial Intelligence.*, 2018, pp. 2079–2086.
- [4] Y. Lin, S. Han, H. Mao, Y. Wang, and W. J. Dally, "Deep gradient compression: Reducing the communication bandwidth for distributed training," *arXiv preprint arXiv:1712.01887*, 2017.
- [5] W. Wen, Y. He, S. Rajbhandari, W. Wang, F. Liu, B. Hu, Y. Chen, and H. Li, "Learning intrinsic sparse structures within long short-term memory," *arXiv preprint arXiv:1709.05027*, 2017.
- [6] S. Hochreiter and J. Schmidhuber, "Long short-term memory," *Neural Computation*, vol. 9, no. 8, pp. 1735–1780, 1997.
- [7] A. Hannun, C. Case, J. Casper, B. Catanzaro, G. Diamos, E. Elsen, R. Prenger, S. Satheesh, S. Sengupta, A. Coates, and A. Y. Ng, "Deep Speech: Scaling up end-to-end speech recognition," *arXiv preprint arXiv:1412.5567*, 2014.
- [8] H. Yin, Z. Wang, and N. K. Jha, "A hierarchical inference model for Internet-of-Things," *IEEE Trans. Multi-Scale Computing Systems*, vol. 4, pp. 260–271, 2018.
- [9] C. Zhu, S. Han, H. Mao, and W. J. Dally, "Trained ternary quantization," *arXiv preprint arXiv:1612.01064*, 2016.
- [10] B. Wu, A. Wan, X. Yue, P. Jin, S. Zhao, N. Golmant, A. Gholaminejad, J. Gonzalez, and K. Keutzer, "Shift: A zero flop, zero parameter alternative to spatial convolutions," in *Proc. IEEE Conf. Computer Vision and Pattern Recognition*, 2018, pp. 9127–9135.
- [11] A. O. Akmandor, H. Yin, and N. K. Jha, "Smart, secure, yet energy-efficient, Internet-of-Things sensors," *IEEE Trans. Multi-Scale Computing Systems*, 2018.
- [12] H. Yin, B. H. Gwee, Z. Lin, A. Kumar, S. G. Razul, and C. M. S. See, "Novel real-time system design for floating-point sub-Nyquist multi-coset signal blind reconstruction," in *Proc. IEEE Int. Symp. Circuits and Systems*, May 2015, pp. 954–957.
- [13] X. Dai, H. Yin, and N. K. Jha, "NeST: A neural network synthesis tool based on a grow-and-prune paradigm," *arXiv preprint arXiv:1711.02017*, 2017.
- [14] S. Han, J. Pool, J. Tran, and W. Dally, "Learning both weights and connections for efficient neural network," in *Proc. Advances in Neural Information Processing Systems*, 2015, pp. 1135–1143.
- [15] T. Zhang, K. Zhang, S. Ye, J. Li, J. Tang, W. Wen, X. Lin, M. Fardad, and Y. Wang, "ADAM-ADMM: A unified, systematic framework of structured weight pruning for DNNs," *arXiv preprint arXiv:1807.11091*, 2018.
- [16] S. Han, J. Kang, H. Mao, Y. Hu, X. Li, Y. Li, D. Xie, H. Luo, S. Yao, Y. Wang, H. Yang, and W. J. Dally, "ESE: Efficient speech recognition engine with sparse LSTM on FPGA," in *Proc. ACM/SIGDA Int. Symp. Field-Programmable Gate Arrays*, 2017, pp. 75–84.
- [17] S. Narang, E. Elsen, G. Diamos, and S. Sengupta, "Exploring sparsity in recurrent neural networks," *arXiv preprint arXiv:1704.05119*, 2017.
- [18] X. Dai, H. Yin, and N. K. Jha, "Grow and prune compact, fast, and accurate LSTMs," *arXiv preprint arXiv:1805.11797*, 2018.
- [19] J. Yu, A. Lukefahr, D. Palframan, G. Dasika, R. Das, and S. Mahlke, "Scalpel: Customizing DNN pruning to the underlying hardware parallelism," *ACM SIGARCH Computer Architecture News*, vol. 45, no. 2, pp. 548–560, 2017.
- [20] K. Cho, B. Van Merriënboer, D. Bahdanau, and Y. Bengio, "On the properties of neural machine translation: Encoder-decoder approaches," *arXiv preprint arXiv:1409.1259*, 2014.
- [21] J. Bradbury, S. Merity, C. Xiong, and R. Socher, "Quasi-recurrent neural networks," *arXiv preprint arXiv:1611.01576*, 2016.
- [22] P. Hill, A. Jain, M. Hill, B. Zamirai, C.-H. Hsu, M. A. Laurenzano, S. Mahlke, L. Tang, and J. Mars, "DeftNN: Addressing bottlenecks for DNN execution on GPUs via synapse vector elimination and near-compute data fission," in *Proc. IEEE/ACM Int. Symp. Microarchitecture*, 2017, pp. 786–799.
- [23] T.-J. Yang, Y.-H. Chen, and V. Sze, "Designing energy-efficient convolutional neural networks using energy-aware pruning," *arXiv preprint arXiv:1611.05128*, 2016.
- [24] X. Dai, P. Zhang, B. Wu, H. Yin, F. Sun, Y. Wang, M. Dukhan, Y. Hu, Y. Wu, Y. Jia, P. Vajda, M. Uyttendaele, and N. K. Jha, "ChamNet: Towards efficient network design through platform-aware model adaptation," *arXiv preprint arXiv:1812.08934*, 2018.
- [25] M. Sandler, A. Howard, M. Zhu, A. Zhmoginov, and L.-C. Chen, "Inverted residuals and linear bottlenecks: Mobile networks for classification, detection and segmentation," *arXiv preprint arXiv:1801.04381*, 2018.
- [26] M. Tan, B. Chen, R. Pang, V. Vasudevan, and Q. V. Le, "MnasNet: Platform-aware neural architecture search for mobile," *arXiv preprint arXiv:1807.11626*, 2018.
- [27] N. Ma, X. Zhang, H.-T. Zheng, and J. Sun, "ShuffleNet V2: Practical guidelines for efficient CNN architecture design," *arXiv preprint arXiv:1807.11164*, 2018.
- [28] S. Narang, E. Undersander, and G. Diamos, "Block-sparse recurrent neural networks," *arXiv preprint arXiv:1711.02782*, 2017.
- [29] "cuSPARSE library," *NVIDIA Corporation, Santa Clara, California*, 2018.
- [30] "cuBLAS library," *NVIDIA Corporation, Santa Clara, California*, 2018.
- [31] G. Chen, B. Wu, D. Li, and X. Shen, "PORPLE: An extensible

- optimizer for portable data placement on GPU," in *Proc. IEEE Int. Symp. Microarchitecture*, 2014, pp. 88–100.
- [32] G. Chen, Y. Zhao, X. Shen, and H. Zhou, "EffiSha: A software framework for enabling efficient preemptive scheduling of GPU," *ACM SIGPLAN Notices*, vol. 52, no. 8, pp. 3–16, 2017.
- [33] "Intel math kernel library," *Intel Corporation, Santa Clara, California*, 2018.
- [34] A. Paszke, S. Gross, S. Chintala, G. Chanan, E. Yang, Z. DeVito, Z. Lin, A. Desmaison, L. Antiga, and A. Lerer, "Automatic differentiation in PyTorch," *NIPS Workshop Autodiff*, 2017.
- [35] M. Zhu and S. Gupta, "To prune, or not to prune: Exploring the efficacy of pruning for model compression," *arXiv preprint arXiv:1710.01878*, 2017.
- [36] M. Marcus, G. Kim, M. A. Marcinkiewicz, R. MacIntyre, A. Bies, M. Ferguson, K. Katz, and B. Schasberger, "The Penn Treebank: Annotating predicate argument structure," in *Proc. Workshop Human Language Technology*, 1994, pp. 114–119.
- [37] S. Merity, N. S. Keskar, and R. Socher, "An analysis of neural language modeling at multiple scales," *arXiv preprint arXiv:1803.08240*, 2018.
- [38] S. Sukhbaatar, A. Szlam, J. Weston, and R. Fergus, "End-to-end memory networks," in *Proc. Advances in Neural Information Processing Systems*, 2015, pp. 2440–2448.
- [39] T. Mikolov, A. Deoras, S. Kombrink, L. Burget, and J. Černocký, "Empirical evaluation and combination of advanced language modeling techniques," in *Proc. Annual Conf. Int. Speech Communication Association*, 2011, pp. 605–608.
- [40] W. Zaremba, I. Sutskever, and O. Vinyals, "Recurrent neural network regularization," *arXiv preprint arXiv:1409.2329*, 2014.
- [41] A. Graves, S. Fernández, F. Gomez, and J. Schmidhuber, "Connectionist temporal classification: Labelling unsegmented sequence data with recurrent neural networks," in *Proc. Int. Conf. Machine Learning*, 2006, pp. 369–376.
- [42] S. Naren, "Speech recognition using DeepSpeech2," <https://github.com/SeanNaren/deepspeech.pytorch/releases>, 2018.
- [43] A. Acero, "Acoustical and environmental robustness in automatic speech recognition," in *Proc. IEEE Int. Conf. Acoustics, Speech, and Signal Processing*, 1990.
- [44] D. Alistarh, D. Grubic, J. Li, R. Tomioka, and M. Vojnovic, "QSGD: Communication-efficient SGD via gradient quantization and encoding," in *Proc. Advances in Neural Information Processing Systems*, 2017, pp. 1709–1720.